Journal of
Intelligent Material
Systems and Structures

Original Article

Journal of Intelligent Material Systems and Structures
2016, Vol. 27(18) 2536–2554

DOI: 10.1177/1045389X16634212
jim.sagepub.com
SAGE

Constitutive modeling of nonlinear reversible and irreversible ferromagnetic behaviors and application to multiferroic composites

Artjom Avakian and Andreas Ricoeur

Abstract

The coupling of magnetic and mechanical fields due to the constitutive behavior of a material is commonly denoted as magnetostrictive effect. The latter is only observed with large coupling coefficients in ferromagnetic materials, where coupling is caused by the rotation of the domains as a result of magnetic (Joule effect) or mechanical (Villari effect) loads. However, only a few elements (e.g. Fe, Ni, Co, and Mn) and their compositions exhibit such a behavior. In this article, the constitutive modeling of nonlinear ferromagnetic behavior under combined magnetomechanical loading as well as the finite element implementation is presented. Both physically and phenomenologically motivated constitutive models have been developed for the numerical calculation of principally different nonlinear magnetostrictive behaviors. On this basis, magnetization, strain, and stress are predicted, and the resulting effects are analyzed. The phenomenological approach covers reversible nonlinear behavior as it is observed, for example, in cobalt ferrite. Numerical simulations based on the physically motivated model focus on the calculation of hysteresis loops and the prediction of local domain orientations and residual stress going along with the magnetization process. Finally, a model for ferroelectric materials is applied in connection with the physically based ferromagnetic approach, in order to predict magnetoelectric coupling coefficients in multifunctional composite.

Keywords

ferromagnetics, magnetostriction, hysteresis loops, nonlinear constitutive modeling, Barkhausen jumps, domain wall motion, multiferroic coupling

Introduction

Ferromagnetic constitutive behavior and motivation

Ferromagnetic behavior has been well known and technically exploited for centuries. Although there are still plenty of research activities in the physics community, the principles of ferromagnetism are well understood nowadays (Bergmann and Schaefer, 2005; Bozorth, 1951; Du Trémolet de Lacheisserie et al., 2005; Kittel, 2006; Morrish, 2001; Stefanita, 2012). For engineering applications, the knowledge of the macroscopic material behavior is in most cases more essential than a deep understanding of the physics on the atomic scale. Magnetostriction is technically exploited in actuation systems, and there are a variety of applications for permanent magnetic fields emanating from poled ferromagnetic devices. New concepts combine ferromagnetic and ferroelectric phases in so-called multiferroic composites (Aboudi, 2001; Bibes and Barthélémy, 2008; Buchanan, 2004; Eerenstein et al., 2007; Fiebig, 2005; Harshe et al., 1993; Hill, 2000; Lu et al., 2011; Nan, 1994; Nan et al., 2008; Ramesh and Spaldin, 2007; Schmid, 1994; Scott, 2007; Van Suchtelen, 1972) in order to induce a coupling of electric and magnetic fields.

All these applications require the knowledge of the constitutive behavior of the employed ferromagnetic material. Therefore, plots of the magnetic induction or magnetization versus the magnetic field are mostly provided by manufacturing companies. The same holds for the strain versus magnetic field curves if the material is suitable for magnetostrictive application. However, stress versus strain characteristics are equally

Institute of Mechanics, University of Kassel, Kassel, Germany

Corresponding author:
Artjom Avakian, Institute of Mechanics, University of Kassel, Monchebergstr. 7, Kassel 34125, Germany.
Email: artjom.avakian@uni-kassel.de

important, however scarcely available. On top of this comes the fact that available plots, especially for hard magnetic materials, mostly are confined just to the quadrant of demagnetization, lacking the full loop.

Some ferromagnetic materials exhibit a pronounced hysteresis behavior; others show an almost reversible nonlinear characteristic. Even two specimens with an identical chemical composition can exhibit qualitatively different features (Bhame and Joy, 2006, 2007, 2008; Borgohain et al., 2010; Concas et al., 2009; El-Okr et al., 2011; Etier et al., 2012; Feltin and Pileni, 1997; Lee et al., 2007; Lu et al., 2007; McCallum et al., 2001; Mohaideen and Joy, 2014; Rajendran et al., 2001; Shi et al., 2000), depending, for example, on the milling of the powder, the sintering conditions, or particle diameters. The reason for the different behaviors is found on the microscale of domain or Bloch walls which are depicted in Figure 1 in connection with a typical plot of magnetization versus magnetic field (Bergmann and Schaefer, 2005; Bozorth, 1951; Du Trémolet de Lacheisserie et al., 2005; Kittel, 2006; Morrish, 2001; Stefanita, 2012). In this article, we refer just to Bloch walls, although Néel walls are likewise observed in ferromagnetic materials (Bergmann and Schaefer, 2005). The presented models are, in principle, applicable to both kinds of domain walls. Néel walls, however, are predominantly found in ferromagnetic thin films, which are not in the focus of our investigations.

In Figure 2, ferromagnetic hysteresis loops in terms of magnetization and magnetostriction versus magnetic field are shown on the left-hand side. In the experiments, specimens of Galfenol have been exposed to combined magnetomechanical loading imposing a compressive stress. In Figure 3, magnetization and engineering strain are plotted versus the magnetic field, here for cobalt ferrite. In contrast to Figure 2, there is almost no hysteresis behavior; in fact, the material shows nearly reversible characteristics. However, cobalt ferrite is also known with pronounced hysteresis behavior if exposed to different manufacturing processes (Bhame and Joy, 2008; Borgohain et al., 2010; El-Okr et al., 2011; Etier et al., 2012; Feltin and Pileni, 1997; Mohaideen and Joy, 2014; Rajendran et al., 2001; Shi et al., 2000).

From the modeling point of view, it is crucial to develop a mathematical framework describing the constitutive behavior of ferromagnetic materials as accurate as possible. Here, both features of reversible and irreversible characteristics have to be covered by different modeling approaches. In connection with a finite element (FE) implementation based on the weak formulation of balance laws, a valuable numerical tool is available to predict the multifield behavior of so-called smart devices and to improve their performance, for example, the magnetoelectric coupling in a multiferroic composite. For such applications, it is inevitable to provide constitutive laws which are thermodynamically consistent, holding for arbitrary combined, for example, magnetomechanical, loading conditions.

In this article, two approaches are presented for the constitutive modeling of ferromagnetic materials. The one is akin to a model for ferroelectrics and is based on microphysical considerations (Avakian et al., 2015; Lange and Ricoeur, 2015). It takes advantage of the fact that some aspects of ferromagnetic and ferroelectric behaviors, although originating from completely different processes on the atomic scale, show comparable features on the meso- and macrolevels. In Figure 2, ferromagnetic and ferroelectric hystereses are compared. Similarities are obvious as well as differences. The ferromagnetic curves exhibit a saturation for larger loads, and the remanent quantities are smaller.

The other approach is purely phenomenological starting from a thermodynamical potential and providing a reversible nonlinear behavior. Both models have been implemented into a FE code to solve complex boundary value problems. In this article, however, the

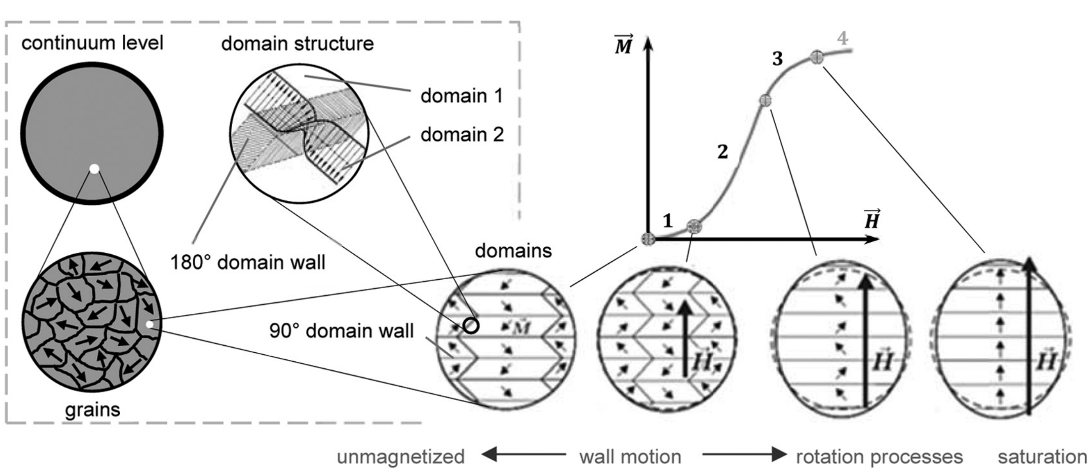

Figure 1. Multiscale effects, Bloch wall motion, and initial magnetization curve for a ferromagnetic material.

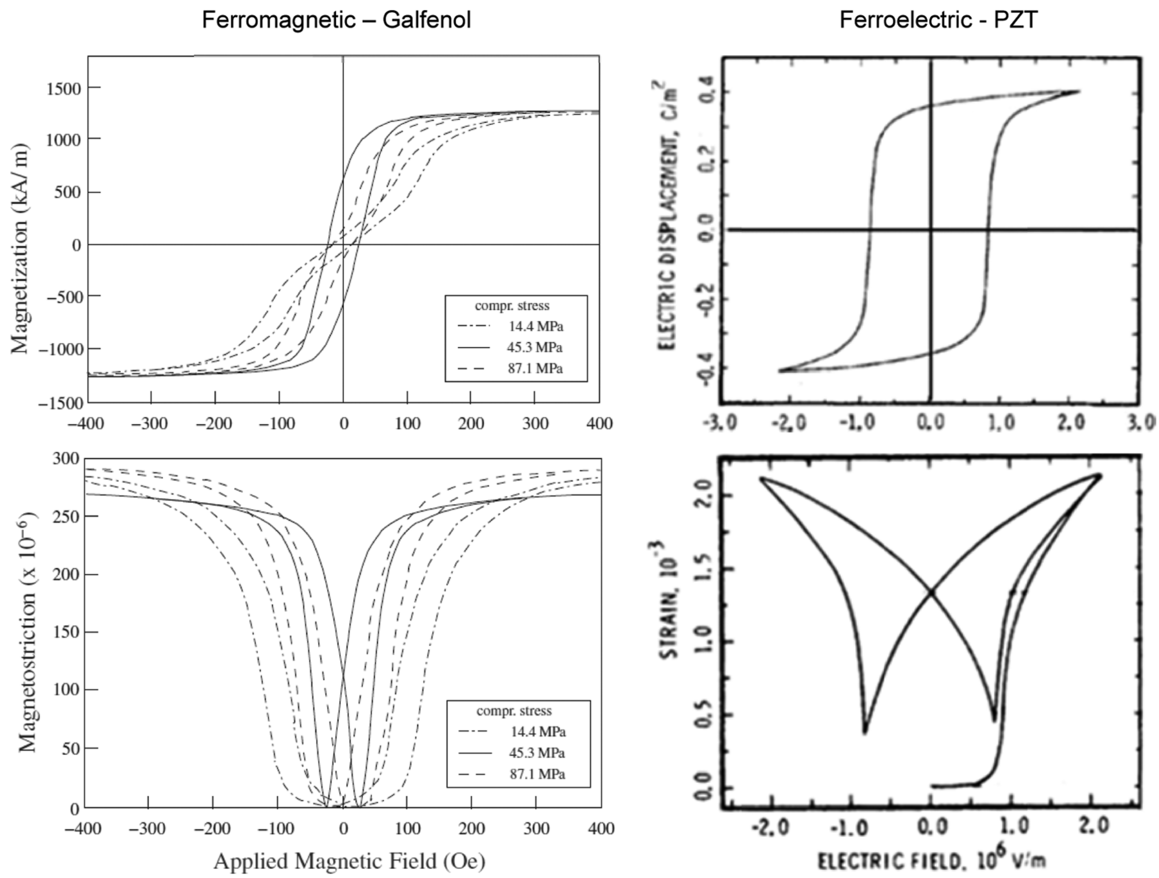

Figure 2. Hysteresis loops: ferromagnetic with combined magnetomechanical loading (left; Kellogg et al., 2005) and ferroelectric with pure electrical loading (right; Chen and Tucker, 1981).

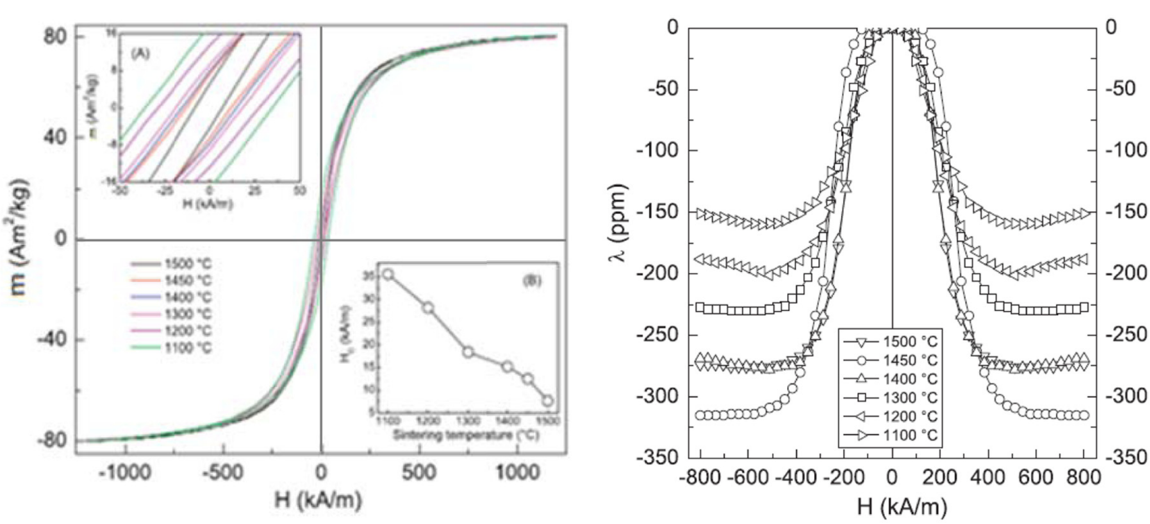

Figure 3. Magnetization and magnetostriction curves of cobalt ferrite at room temperature as a function of magnetic field for samples sintered at different temperatures (Mohaideen and Joy, 2014).

focus is on the constitutive behavior, demonstrated at simple bulk specimens under uni- or multiaxial magnetomechanical loadings. Both models will not be able to cover the whole variety of sophisticated features of ferromagnetic behavior in detail, which may arise or disappear due to slight differences in material processing. The goal is rather to provide constitutive frameworks reflecting the essential features such as saturation, remanence, and dissipation and their dependence on external loading conditions or kinematical constraints. Finally, an applied example is shown solving the boundary value problem of a multiferroic particle composite, accounting for ferromagnetic and ferroelectric constitutive models, yielding the magnetoelectric coupling coefficient versus the applied magnetic field.

State of the art

Linear constitutive modeling of magnetoelasticity is still common in the solid mechanics community and considered to be appropriate in many applications (Aboudi, 2001; Buchanan, 2004; Labusch et al., 2014; Lee et al., 2005; Nan, 1994; Tang and Yu, 2009; Wan et al., 2003). Analytical solutions, for example, in order to determine effective properties of composites with magnetic constituents (Benveniste, 1995; Huang and Kuo, 1997; Krantz and Gerken, 2013; Kuo et al., 2010; Li, 2000; Li and Dunn, 1998), are in general only feasible if based on a linear constitutive framework. The interpretation of the results, however, requires the introduction of a bias magnetic field as the center of a local tangent, holding for sufficiently small perturbations.

A classical phenomenological approach to describe general hysteresis behavior is based on the Preisach (1935) model which has originally been formulated in a scalar notation and much later been generalized within a tensorial framework to cover multidimensional problems (Mayergoyz and Friedman, 1987). The basic idea behind the Preisach model is that smooth hysteresis loops as observed experimentally are actually the result of a large number of elementary hysterons being subject to a weighted averaging. The approach has subsequently been applied to ferromagnetic materials (Adly et al., 1991; Bergqvist and Engdahl, 1991; Cardelli et al., 2004; Kádár, 1987; Restorff et al., 1990).

The Jiles-Atherton (1995) model has been developed to specifically describe ferromagnetic hysteresis behavior. Also, originally starting from a one-dimensional formulation, more general approaches have been following (Bergqvist, 1996; Dapino et al., 2000). The model holds both physical and phenomenological aspects. Domain wall bowing and domain wall motion, the latter impeded by defects, are distinguished to introduce reversible and irreversible contributions to the magnetization. While the irreversible losses are calculated from an energy balance, the nonlinear reversible contribution may be formulated phenomenologically.

Statistical mechanics is applied in the Armstrong (1997, 2003) model to calculate magnetization and magnetostriction. The hysteresis behavior is introduced in a way similar to the Jiles-Atherton model by minimizing the local internal energy in connection with a probability density function leading to an evolution of domain volume fractions. Energy losses are again associated with impediments to domain wall motion, for example, due to point defects. Applications of the model to other ferromagnetic materials are found in Atulasimha et al. (2007) and Evans and Dapino (2010).

A more general approach to ferroic materials has been suggested by Smith et al. (2006). Although from the mathematical point of view, the model is akin to the Preisach model, assuming that the macroscopic hysteresis curves are the results of statistically distributed elementary hysterons, the approach has a strong physical basis. Applied to ferromagnetic materials within a scalar framework (Smith and Dapino, 2006), the hysteron or kernel considers the exchange energy and the work of a magnetic field on the lattice scale. Rate dependence is introduced with Boltzmann statistics, and the total magnetization is determined by stochastic homogenization. Since physical effects are included in the kernel, the hysteresis loops from the homogenized energy model show better agreement with experiments than those emanating from the classical Preisach model with kernels containing simple weights or density functions.

The phase field approach, for the past 15 years having experienced a continuous increase in popularity in various fields of application, has also been exploited toward modeling ferromagnetic materials (Entel et al., 2006; Koyama, 2008; Koyama and Onodera, 2003; Lu et al., 2009, 2011; Ma et al., 2014; Miehe and Ethiraj, 2012; Zayak et al., 2002). Based on an energy functional and the Ginzburg–Landau equation, corresponding to subcritical bifurcation and being derived from a Landau–Lifshitz–Gilbert equation of motion of the magnetization in a one-dimensional uniaxial ferromagnet, the domain wall motion is calculated in terms of an evolution of phase fields.

Phenomenological constitutive models, adapting multiple empirical parameters to experimental findings, have been developed with and without internal variables, in order to describe irreversible (Carman and Mitrovic, 1995; Kiefer and Lagoudas, 2004; Linnemann et al., 2009; Miehe et al., 2011a, 2011b; Xu et al., 2013) or reversible ferromagnetic and magnetostrictive behavior. Concerning models for the nonlinear reversible behavior, being one part of this article, the simplest extension of linearity is given by the standard square model (Carman and Mitrovic, 1995; Wan et al., 2003; Wan and Zhong, 2004). It is capable of describing the symmetry of strain with respect to a change of sign in the magnetic field and the zero gradient for vanishing fields however fails to reproduce the saturation for larger magnetic loads. Concerning models with saturation (Wan et al., 2003), two approaches are suggested, the so-called hyperbolic tangent (HT) model and the density of domain switching (DDS) model. While the HT overestimates the magnetostriction by 40%, the DDS leads to its underestimation by up to 30%, depending on the mechanical pre-load. In Zheng and Liu (2005), a model is presented, which is in good agreement with experimental findings; however, different ranges of the curves are described by separate equations. None of these articles deals with a general multiaxial tensorial representation of the constitutive equations or a FE implementation within an electro-magneto-mechanical framework. Moreover, the material laws have specifically been developed and verified for the behavior of Terfenol-D.

Constitutive behavior: comparison of modeling approaches

Before presenting the modeling approaches in detail, the constitutive frameworks of ferroelectric and reversible and irreversible ferromagnetic behaviors are summarized and compared to each other. Ferroelectric materials exposed to electromagnetic fields are described by the following constitutive equations (Avakian et al., 2015)

$$\begin{aligned} \sigma_{ij} &= c_{ijkl}\left(\varepsilon_{kl} - \varepsilon_{kl}^{irr}\right) - e_{lij}E_l, \\ D_l &= e_{lij}\left(\varepsilon_{ij} - \varepsilon_{ij}^{irr}\right) + \kappa_{ln}E_n + P_l{}^{irr} \\ B_k &= \mu_{km}H_m. \end{aligned} \tag{1}$$

Within a microphysical framework, the irreversible strain ε_{kl}^{irr} and polarization P_l^{irr} are due to domain wall motion. Considering plane problems, a grain consists of four domain species separated by 90°- and 180°-domain walls. The formulation of a nonlinear constitutive law thus requires four internal variables and associated evolution equations describing the switching of unit cells on the microlevel. Due to intended applications within a multiferroic framework, the ferroelectric material is allocated a magnetic permeability expressed by the third equation relating the magnetic field H_m and the induction B_k. The elastic, piezoelectric, dielectric, and magnetic permeability tensors c_{ijkl}, e_{lij}, κ_{ln}, and μ_{km} also depend on the internal variables, giving rise to an additional source of nonlinearity, even in the magnetic properties. The other quantities in equation (1) are stress σ_{ij}, electric field E_l, and electric displacement D_l.

Based on the same ideas as in equation (1), the ferromagnetic constitutive equations read

$$\begin{aligned} \sigma_{ij} &= c_{ijkl}\left(\varepsilon_{kl} - \varepsilon_{kl}^{irr}\right), \\ D_l &= \kappa_{ln}E_n, \\ B_k &= \mu_{km}H_m + M_k^{irr}. \end{aligned} \tag{2}$$

Here, irreversible strain and irreversible magnetization M_k^{irr} or magnetic polarization, respectively, are likewise governed by four internal variables describing Bloch wall motion due to magnetomechanical driving forces. In Figure 1, a typical domain structure of ferromagnetic material is depicted, showing four species in regions 1 and 2, two of them vanishing at larger fields. The affinity to ferroelectricity on the macro- and mesoscales allows for a similar modeling of ferromagnetism covering the essential phenomena. Figure 1 also illustrates the physics on the microscale close to a Bloch wall, featuring a continuous rotation of atomic magnets rather than a switching of unit cells. Anyway, in the constitutive framework, both physical processes merge into an evolution law for the internal variables, which is based on the magnetoelastic or electroelastic energies, respectively, going along with the changes of the directions of magnetic or electric dipoles.

In contrast to ferroelectricity, piezomagnetic coefficients relating magnetic field and stress or strain and magnetic induction are not involved, accounting for the saturation depicted in Figure 2. As a second consequence, the irreversible strain does not directly induce a magnetic induction B_k. Magnetostriction is rather induced by the irreversible part of the strain, which in turn is controlled not only by the magnetic field but also by mechanical loads. The same way, a strain field has an impact on the magnetic induction via M_k^{irr}. Dielectric properties are allocated by the second equation in equation (2) which is linear only at the first glance since the dielectric constants κ_{ln} are controlled by the internal variables in a nonlinear manner. Ferromagnetic materials exhibiting a significant electric conductivity are excluded by the model.

While equation (2) generates hysteresis loops, the constitutive equations of nonlinear reversible ferromagnetic behavior are given by

$$\begin{aligned} \dot{\sigma}_{ij} &= c_{ijkl}(\varepsilon_{kl}, H_k)\dot{\varepsilon}_{kl} - q_{kij}(\varepsilon_{kl}, H_k)\dot{H}_k, \\ \dot{D}_l &= \kappa_{ln}\left(\varepsilon_{ij}, H_k\right)\dot{E}_n, \\ \dot{B}_k &= q_{kij}\left(\varepsilon_{ij}, H_m\right)\dot{\varepsilon}_{ij} + \mu_{km}\left(\varepsilon_{ij}, H_m\right)\dot{H}_m, \end{aligned} \tag{3}$$

where a rate-dependent depiction has been chosen. The nonlinearity is completely included in the material coefficients depending on the independent variables strain and magnetic field. Due to the reversibility of the constitutive behavior, these functions are unique, not involving any internal variables. The coefficient functions, now including the magnetostrictive tensor $q_{kij}(\varepsilon_{kl}, H_k)$, have to be chosen in a way to reflect experimental observations. A second requirement is to satisfy thermodynamical consistency by defining a thermodynamical potential yielding all the coefficient functions by differentiation. These purely phenomenological approaches involve several parameters, which are adjusted to specific material behaviors.

Constitutive models of ferromagnetic materials

Physically motivated ferromagnetic model

For the electro- and magnetostatic case ($\dot{\vec{B}}, \dot{\vec{D}} = 0$), the scalar electric and magnetic potentials φ^{el} and φ^{m} are motivated from the two Maxwell equations, that is, Faraday's and Ampere's Laws (Jackson, 1998). Their gradients yield electric and magnetic fields (Vanderlinde, 2005), just as displacements u_i and strain are related for infinitely small deformations

$$\varepsilon_{ij} = \frac{1}{2}\left(u_{i,j} + u_{j,i}\right),\ E_k = -\varphi^{el}_{,k},\ H_l = -\varphi^{m}_{,l}. \tag{4}$$

To define boundary value problems in a strict formulation, the balance equation of momentum

$$\sigma_{ij,j} + b_i = \rho\ddot{u}_i = 0 \tag{5}$$

has to be considered besides the other two Maxwell equations, that is, Gauss' Law and Gauss' Magnetism Law. The quasi-static limit is prescribed neglecting inertia effects and b_i stands for the specific body forces. Since free electric volume charges are assumed not to be present in a dielectric material and volume forces are commonly neglected ($b_i = 0$), the balance equations can be specified as

$$\sigma_{ij,j} = 0,\ D_{l,l} = 0,\ B_{k,k} = 0. \tag{6}$$

Cauchy's theorem, introducing tractions t_i, is generalized providing the relations

$$t_i = \sigma_{ij}n_j,\ \omega^{el}_s = -D_k n_k,\ \omega^m_s = -B_l n_l, \tag{7}$$

where ω^{el}_s is the surface charge density and ω^m_s is the part of the magnetic flux along the surface normal n_l of the Neumann-type boundary S_ω.

Reversible quantities will from now on be denoted with a superscript "r." According to a common approach, strain ε_{ij} and magnetic induction B_k are additively decomposed into reversible and irreversible parts

$$\varepsilon_{ij} = \varepsilon^r_{ij} + \varepsilon^{irr}_{ij},\ B_k = B^r_k + M^{irr}_k. \tag{8}$$

The irreversible parts are due to Barkhausen jumps on the microlevel or domain wall motion on the mesoscopic level (see Figure 1). It should be noted that a reversibility of ε^r_{ij} and B^r_k at this point disregards changes of effective material properties which are, however, incorporated in the implementation. Concerning the electric displacement, just these weak nonlinearities are present due to changes of the dielectric constants κ_{ln} in equation (2) as a consequence of Bloch wall motion, while an explicit nonlinearity due to polarization rearrangement does not exist, that is, $P^{irr}_l = 0$.

The specific Helmholtz free energy f (Cocks and McMeeking, 1999) is also decomposed as

$$f\left(\varepsilon_{ij}, D_k, B_l\right) = f^r\left(\varepsilon^r_{ij}, D^r_l, B^r_k\right) + f^{irr}\left(\varepsilon^{irr}_{ij}, M^{irr}_k\right), \tag{9}$$

where f^r and f^{irr} are the reversible and irreversible parts. f^{irr} depends on irreversible strain and magnetization and thus on the internal variables of a constitutive model. The exchange rate of the free energy is obtained from the total differential of equation (9) where the associated variables σ_{ij}, H_k and E_l are obtained by partial differentiation of the potential with respect to the independent variables (Parton and Kudryavtsev, 1988)

$$\begin{aligned}\dot{f}\left(\dot{\varepsilon}_{ij}, \dot{D}_l, \dot{B}_k\right) &= \dot{f}^r\left(\dot{\varepsilon}^r_{ij}, \dot{D}^r_l, \dot{B}^r_k\right) + \dot{f}^{irr}\left(\dot{\varepsilon}^{irr}_{ij}, \dot{M}^{irr}_k\right)\\ &= \sigma_{ij}\left(\dot{\varepsilon}^r_{ij} + \dot{\varepsilon}^{irr}_{ij}\right) + E_l\dot{D}^r_l + H_k\left(\dot{B}^r_k + \dot{M}^{irr}_k\right).\end{aligned} \tag{10}$$

The choice of strain and electric and magnetic fields as independent variables is more feasible for engineering applications; thus, the constitutive ferromagnetic model is based on the thermodynamical potential $\Psi(\varepsilon_{ij}, E_l, H_k)$. Applying a Legendre transformation, that is

$$\begin{aligned}\Psi\left(\varepsilon_{ij}, E_l, H_k\right) &= f\left(\varepsilon_{ij}, D_l, B_k\right) - \frac{\partial f}{\partial D_l}D_l - \frac{\partial f}{\partial B_k}B_k,\\ &= f - E_l D_l - H_k B_k\end{aligned} \tag{11}$$

the rate-dependent formulation is derived inserting equation (10)

$$\begin{aligned}d\Psi &= \sigma_{ij}d\varepsilon_{ij} - D_l dE_l - B_k dH_k\\ &= \sigma_{ij}\left(d\varepsilon^r_{ij} + d\varepsilon^{irr}_{ij}\right) - D^r_l dE_l - \left(B^r_k + M^{irr}_k\right)dH_k.\end{aligned} \tag{12}$$

Integrating the infinitesimal changes of state, the thermodynamical potential is obtained as

$$\begin{aligned}\Psi\left(\varepsilon_{ij}, E_l, H_k\right) &= \frac{1}{2}c_{ijkl}\varepsilon_{kl}\varepsilon_{ij} - \frac{1}{2}\kappa_{ln}E_l E_n\\ &- \frac{1}{2}\mu_{km}H_k H_m - c_{ijkl}\varepsilon^{irr}_{kl}\varepsilon_{ij} - M^{irr}_k H_k.\end{aligned} \tag{13}$$

The constitutive equations of nonlinear ferromagnetic behavior within a magnetoelectric context are then given by

$$\begin{aligned}\sigma_{ij} &= \left.\frac{\partial\Psi\left(\varepsilon_{ij}, E_l, H_k\right)}{\partial\varepsilon_{ij}}\right|_{E_l, H_k} = c_{ijkl}\left(\varepsilon_{kl} - \varepsilon^{irr}_{kl}\right),\\ D_l &= -\left.\frac{\partial\Psi\left(\varepsilon_{ij}, E_l, H_k\right)}{\partial E_l}\right|_{\varepsilon_{ij}, H_k} = \kappa_{ln}E_n,\\ B_k &= -\left.\frac{\partial\Psi\left(\varepsilon_{ij}, E_l, H_k\right)}{\partial H_k}\right|_{\varepsilon_{ij}, E_l} = \mu_{km}H_m + M^{irr}_k,\end{aligned} \tag{14}$$

which coincide with equation (2) from the compilation in section "Constitutive behavior: comparison of modeling approaches." Relating the third constitutive equation to common representations in textbooks, the irreversible magnetization M^{irr}_k is in a more general

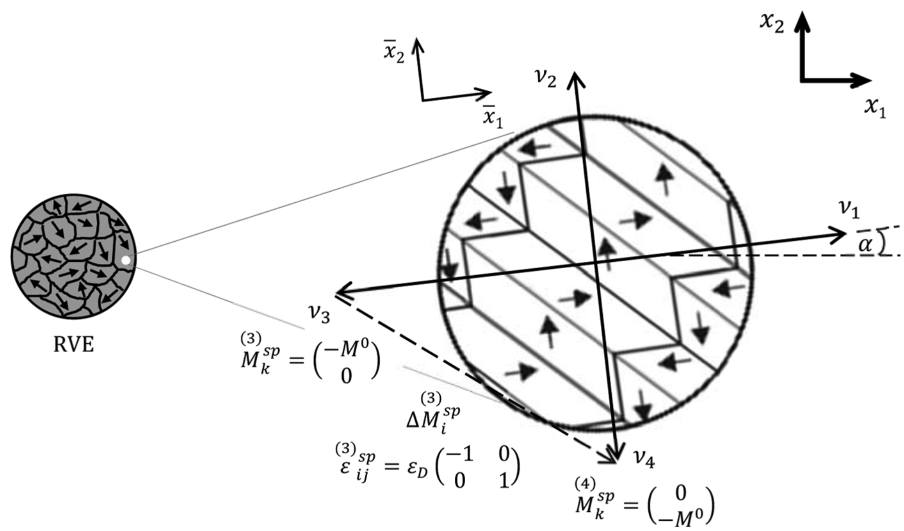

Figure 4. Internal variables ν_n and the magnetic orientations in a grain with local coordinate system $(\bar{x}_1, \bar{x}_2)$. Characterization of the orientation of domain variants $n = 1, \ldots, 4$ with respect to the global coordinate system (x_1, x_2) by an angle α.

sense denoted as spontaneous magnetic polarization or magnetization M_k^{sp}

$$B_k = \mu_0(\delta_{km} + \chi_{km})H_m + M_k^{sp} = \mu_0\mu_{km}^r H_m + M_k^{sp} = \mu_{km}H_m + M_k^{sp}, \qquad (15)$$

where δ_{km} is the Kronecker identity tensor, χ_{km} is the magnetic susceptibility, μ_0 is the magnetic permeability of vacuum, and μ_{km}^r are the coefficients of relative permeability of the material (≥ 1).

On the continuum level, domain wall motion is described by internal variables ν_n (see Figure 4) for plane problems associated with the four possible orientations of domains in a grain (see Figure 1) with the easy axis in the $\langle 100 \rangle$ direction (Bergmann and Schaefer, 2005; Du Trémolet de Lacheisserie et al., 2005; Kittel, 2006; Morrish, 2001)

$$\dot{\varepsilon}_{ij}^{irr} = \sum_{n=1}^{4} \overset{(n)}{\varepsilon}{}_{ij}^{sp}\, \dot{\nu}_n, \; \dot{M}_k^{irr} = \sum_{n=1}^{4} \Delta \overset{(n)}{M}{}_k^{sp}\, \dot{\nu}_n, \qquad (16)$$

where $\overset{(n)}{\varepsilon}{}_{ij}^{sp}$ and $\Delta \overset{(n)}{M}{}_k^{sp}$ represent the spontaneous strain and change of spontaneous magnetization for the domain n, respectively. The total change of volumes of the domain species in a grain resulting from Bloch wall motion is conserved by the following relations

$$0 \leq \nu_n \leq 1, \; \sum_{n=1}^{4} \nu_n = 1, \qquad (17)$$

where ν_n stands for the specific volume of each domain. In all calculations, the generalized state of plane stress will be assumed, that is, $\sigma_{i3} = 0$, $D_3 = 0$, and $B_3 = 0$. The changes of magnetization exhibit three possibilities, $\pm 90°$ and $180°$, for each domain species $n = 1, \ldots, 4$. In Figure 4, one variant for $n = 3$ is depicted as an example, that is, $\Delta \overset{(3)}{M}{}_k^{sp} = \overset{(4)}{M}{}_k^{sp} - \overset{(3)}{M}{}_k^{sp}$ for $+90°$ jumping. Concerning the spontaneous strain, each domain species ν_n is allocated one unique tensor representing $\pm 90°$ jumping.

The rates of volume change of the species $\dot{\nu}_n$, that is, the time derivatives of the internal variables, play an important role in the thermodynamical formulation of the material law. The evolution of the internal variables ν_n within a domain structure is controlled by an energetic criterion, which has been chosen in the style of ferroelectric switching criteria (Hwang et al., 1995; Kessler and Balke, 2001)

$$\Delta w^n = \sigma_{ij} \overset{(n)}{\varepsilon}{}_{ij}^{sp} + H_k \Delta \overset{(n)}{M}{}_k^{sp} \geq w^{crit} \qquad (18)$$

The left-hand side of the inequality, consisting of mechanical and magnetic contributions, represents the dissipative work Δw^n of Bloch wall motion due to the jumping of a species n.

Barkhausen jumping occurs when the dissipative energy exceeds an associated critical value w^{crit}. In plane, there are three possible jumping variants with the easy axis in the $\langle 100 \rangle$ direction. Based on the idea of ferroelectric switching (Hwang et al., 1995; Kamlah et al., 2005), two different threshold values have to be introduced

$$w^{crit} = \begin{cases} \sqrt{2}M^0 H_c & \pm 90° \\ 2M^0 H_c & 180° \end{cases}, \qquad (19)$$

where the material parameters H_c and M^0 are coercive field and magnitude of spontaneous magnetization.

On the macroscopic level, an evolution law for the internal variables ν_n controls Bloch wall motion. Based on equations (18) and (19), the evolution law for a domain species n is

$$\dot{\nu}_n = -\dot{\nu}_n^0 \mathcal{H}\left(\frac{\Delta\tilde{w}^n}{w^{crit}} - 1\right),\ \Delta\tilde{w}^n = \max\left(\Delta w^n_{\pm 90°}, \Delta w^n_{180°}\right), \tag{20}$$

where $\mathcal{H}(..)$ is the Heaviside function and $\dot{\nu}_n^0$ is a model parameter. The latter represents a discrete amount of domain wall motion, which has to be chosen within a numerical context. Equation (20) determines whether the volume of the species n decreases by a magnitude $d\nu_n^0$ due to local jumping or not. The reduction of ν_n always occurs in favor of another species, satisfying equation (17).

To prove the thermodynamical consistency of the evolution law equation (20), the second law of thermodynamics is formulated as

$$\theta\dot{s} + \theta\frac{\partial}{\partial x_i}\left(\frac{q_i}{\theta}\right) - \rho r \geq 0, \tag{21}$$

where s represents the specific entropy and θ the absolute thermodynamic temperature, q_i/θ is the entropy flow through the surface of the control volume, and ρr is a volume heat source. The generalized Clausius–Duhem inequality for thermo-ferromagnetic material behavior is finally obtained from equation (21) reading (see Avakian et al., 2015, for a similar derivation)

$$\underbrace{\sigma_{ij}\dot{\varepsilon}_{ij}^{irr} + H_k\dot{M}_k^{irr}}_{\dot{w}} - \frac{q_i}{\theta}\frac{\partial\theta}{\partial x_i} \geq 0. \tag{22}$$

The irreversible changes of states $\dot{\varepsilon}_{ij}^{irr}$ and $\dot{M}_k^{irr}$, being weighted averages in each grain, are defined according to equation (16). Disregarding heat flux, that is, $q_i = 0$, equation (22) means that the power $\dot{w}$ associated with the driving forces of domain action always has to be positive. Relating equation (22) to a specific domain species n within a grain, the generalized Clausius–Duhem inequality equation (22) is modified as

$$\underbrace{\sigma_{ij}\overset{(n)}{\varepsilon}{}_{ij}^{sp} + H_k\Delta\overset{(n)}{M}{}_k^{sp}}_{\Delta w^n} - \frac{q_i}{\theta}\frac{\partial\theta}{\partial x_i} \geq 0. \tag{23}$$

Assuming isothermal or adiabatic conditions, that is, $\theta_{,i} = 0$, equation (23) claims the jumping work Δw^n to be always positive, thus implying thermodynamical consistency of the switching criterion equation (18) and thus the evolution equation (20). It has to be noted that equation (22) neglects irreversibilities due to changes in materials properties, whereupon, for example, dielectric fields remain entirely disregarded in the Clausius–Duhem inequality. The dissipation from Bloch wall motion, however, is much larger than the one from the evolution of material tangents.

While the changes of strain and spontaneous magnetization due to Bloch wall motion are described by equation (16), the evolution of material tangents in an representative volume element (RVE) or grain is likewise connected to the internal variables

$$c_{ijkl} = \sum_{n=1}^{4} \overset{(n)}{c}_{ijkl}\nu_n \rightarrow \dot{c}_{ijkl} = \sum_{n=1}^{4} \overset{(n)}{c}_{ijkl}\dot{\nu}_n = \sum_{n=1}^{4} \frac{\partial c_{ijkl}}{\partial \nu_n}\dot{\nu}_n \tag{24}$$

and similar

$$\kappa_{ln} = \sum_{n=1}^{4} \overset{(n)}{\kappa}_{ln}\,\nu_n,\ \mu_{km} = \sum_{n=1}^{4} \overset{(n)}{\mu}_{km}\nu_n. \tag{25}$$

Phenomenologically motivated ferromagnetic model

The constitutive behavior of the ferromagnetic–dielectric material is assumed to be governed by the thermodynamic potential

$$\begin{aligned}\bar{\Psi}(\sigma_p, E_l, H_k) = &-\frac{1}{2}s_{11}\sigma_1\sigma_1 - s_{12}\sigma_1\sigma_2\\ &-\frac{1}{2}s_{22}\sigma_2\sigma_2 - s_{66}\sigma_6\sigma_6 - \frac{1}{2}\kappa_{11}E_1E_1\\ &-\frac{1}{2}\kappa_{22}E_2E_2 - \frac{1}{2}\bar{\mu}_{11}^0 H_1H_1 - \frac{\eta_1}{1+\zeta_1H_1^{-3}}\sigma_1\\ &-\frac{\eta_2}{1+\zeta_2H_1^{-3}}\sigma_2 - \rho\{H_1 - \xi\ln(\xi + H_1)\},\end{aligned} \tag{26}$$

where stress and electric and magnetic fields are chosen as independent variables. It is feasible to develop the material model based on stress and magnetic field since these are the quantities which are commonly controlled in experiments. In this section, the Voigt notation is applied to higher-order tensors, so, for example, σ_6 is the shear stress σ_{12}. Essential features of magnetization and magnetostriction are appropriately described adapting the constant coefficients η_i, ζ_i, ρ, and ξ to experimental curves. Equation (26) has been formulated in a local coordinate system where the x_1-axis is attached to the vector of the H field. Thus, H_2 does not appear in the potential. The easy axis locally always points in the direction of the magnetic field since the reversibility, in connection with a vanishing remanence, leads to an immediate magnetization even at low field intensities. Thus, the x_1-axes of the local coordinate systems are always attached to the direction of magnetization, and the material tensors are sparsely populated in these coordinate systems. The dielectric properties, for example, are represented just by κ_{11} and κ_{22}. The potential according to equation (26), being valid locally and adjusted to the local coordinates, thus contains only these coefficients. In global coordinates, to which all results are related, the material tensors in general are fully populated.

The superscript in the magnetic permeability $\bar{\mu}_{11}^0$ indicates a constant magnitude in contrast to the function $\bar{\mu}_{11}(\sigma_p, H_k)$. The denominators in equation (26) cannot be zero since ζ_1 and ζ_2 are always positive, requiring a negative value of H_1 for a division by zero. This is not possible, however, since the local coordinate system is always adapted to the H-field such that $H_1>0$. The general constitutive behavior is obtained by differentiation of equation (26) according to

$$\begin{aligned}\dot{\varepsilon}_p\left(\dot{\sigma}_q, \dot{E}_l, \dot{H}_k\right) &= \frac{-\partial^2\bar{\Psi}}{\partial\sigma_p\partial\sigma_q}\dot{\sigma}_q + \frac{-\partial^2\bar{\Psi}}{\partial\sigma_p\partial E_l}\dot{E}_l + \frac{-\partial^2\bar{\Psi}}{\partial\sigma_p\partial H_k}\dot{H}_k,\\ \dot{D}_l\left(\dot{\sigma}_p, \dot{E}_n, \dot{H}_k\right) &= \frac{-\partial^2\bar{\Psi}}{\partial E_l\partial\sigma_p}\dot{\sigma}_p + \frac{-\partial^2\bar{\Psi}}{\partial E_l\partial E_n}\dot{E}_n + \frac{-\partial^2\bar{\Psi}}{\partial E_l\partial H_k}\dot{H}_k,\\ \dot{B}_k\left(\dot{\sigma}_p, \dot{E}_l, \dot{H}_m\right) &= \frac{-\partial^2\bar{\Psi}}{\partial H_k\partial\sigma_p}\dot{\sigma}_p + \frac{-\partial^2\bar{\Psi}}{\partial H_k\partial E_l}\dot{E}_l + \frac{-\partial^2\bar{\Psi}}{\partial H_k\partial H_m}\dot{H}_m\end{aligned} \tag{27}$$

where the material coefficients, for example, the compliances s_{11} and s_{12}, are assumed to be constant within incremental changes of state, and thus, the rate-dependent constitutive framework is given by

$$\begin{aligned}\dot{\varepsilon}_p\left(\dot{\sigma}_q, \dot{H}_k\right) &= s_{pq}\dot{\sigma}_q + \bar{q}_{kp}(H_k)\dot{H}_k,\\ \dot{D}_l\left(\dot{E}_n\right) &= \kappa_{ln}\dot{E}_n,\\ \dot{B}_k\left(\dot{\sigma}_p, \dot{H}_m\right) &= \bar{q}_{kp}(H_m)\dot{\sigma}_p + \bar{\mu}_{km}\left(\sigma_p, H_m\right)\dot{H}_m.\end{aligned} \tag{28}$$

Equation (28) represents nonlinear but, in contrast to the microphysical model, reversible changes of state since the material tensors are unique functions of the independent variables. The electric displacement just depends on the electric field, in a ferromagnetic material not being coupled with mechanical or magnetic fields. A bar is added to the magnetic permeability $\bar{\mu}_{km}(\sigma_p, H_m)$ and magnetostrictive coefficients $\bar{q}_{kp}(H_k)$ to distinguish from quantities based on a different potential. Equation (28) due to the tensorial representation allowing for multiaxial loading, the responses, for example, in the x_1-direction is obtained as

$$\dot{\varepsilon}_1\left(\dot{\sigma}_q, \dot{H}_k\right) = s_{11}\dot{\sigma}_1 + s_{12}\dot{\sigma}_2 + 3\frac{\eta_1\zeta_1H_1^2}{\left(\zeta_1 + H_1^3\right)^2}\dot{H}_1, \tag{29}$$

$$\dot{D}_1\left(\dot{E}_n\right) = \kappa_{11}\dot{E}_1, \tag{30}$$

$$\dot{B}_1\left(\dot{\sigma}_p, \dot{H}_m\right) = 3\frac{\eta_1\zeta_1H_1^2}{\left(\zeta_1 + H_1^3\right)^2}\dot{\sigma}_1 + 3\frac{\eta_2\zeta_2H_1^2}{\left(\zeta_2 + H_1^3\right)^2}\dot{\sigma}_2. + \left(\bar{\mu}_{11}^0 + \frac{6\eta_1\zeta_1H_1\left(\zeta_1 - 2H_1^3\right)\sigma_1}{\left(\zeta_1 + H_1^3\right)^3} + \frac{6\eta_2\zeta_2H_1\left(\zeta_2 - 2H_1^3\right)\sigma_2}{\left(\zeta_2 + H_1^3\right)^3} + \frac{\rho\xi}{\left(\xi + H_1\right)^2}\right)\dot{H}_1. \tag{31}$$

In general, all material coefficients depend on the three independent variables. Experimental observations, however, put this thermodynamical requirement into perspective, showing, for example, a noticeable nonlinearity of the stress–strain curve only for giant magnetostrictive materials. In the potential equation (26) and the constitutive relation equation (28), the magnetostrictive constants are functions of just the magnetic field, and the magnetic permittivity is a function of both magnetic field and stress

$$\bar{q}_{11} = 3\frac{\eta_1\zeta_1H_1^2}{\left(\zeta_1 + H_1^3\right)^2}, \quad \bar{q}_{12} = 3\frac{\eta_2\zeta_2H_1^2}{\left(\zeta_2 + H_1^3\right)^2} \tag{32}$$

$$\bar{\mu}_{11} = \bar{\mu}_{11}^0 + \frac{6\eta_1\zeta_1H_1\left(\zeta_1 - 2H_1^3\right)\sigma_1}{\left(\zeta_1 + H_1^3\right)^3} + \frac{6\eta_2\zeta_2H_1\left(\zeta_2 - 2H_1^3\right)\sigma_2}{\left(\zeta_2 + H_1^3\right)^3} + \frac{\rho\xi}{\left(\xi + H_1\right)^2}. \tag{33}$$

A more sophisticated model replaces the constant coefficients ζ_1, ζ_2, and ξ by variables depending on the stresses

$$\begin{aligned}&\zeta_1 = \zeta_1^0 + \zeta_1^\sigma(\sigma_1 - \sigma_2), \quad \zeta_2 = \zeta_2^0 + \zeta_2^\sigma(\sigma_1 - \sigma_2),\\ &\xi = \xi^0 + \xi^\sigma(\sigma_1 - \sigma_2).\end{aligned} \tag{34}$$

Both variants of the phenomenological constitutive model will be investigated in section "Results." For the numerical implementation, the independent mechanical variable is changed from stress to strain. Accordingly, the material tensors are subject to the following transformations

$$c_{pq} = s_{pq}^{-1}, \; q_{kp} = \bar{q}_{kq}c_{qp}, \; \mu_{km} = \bar{\mu}_{km} - \bar{q}_{kq}c_{qp}\bar{q}_{mp}. \tag{35}$$

The constitutive equations for the nonlinear reversible ferromagnetic behavior are thus given as

$$\begin{aligned}\dot{\sigma}_p\left(\dot{\varepsilon}_q, \dot{H}_k\right) &= c_{pq}\dot{\varepsilon}_q - q_{kp}\left(\varepsilon_q, H_k\right)\dot{H}_k,\\ \dot{D}_l\left(\dot{E}_n\right) &= \kappa_{ln}\dot{E}_n,\\ \dot{B}_k\left(\dot{\varepsilon}_p, \dot{H}_m\right) &= q_{kp}\left(\varepsilon_p, H_m\right)\dot{\varepsilon}_p + \mu_{km}\left(\varepsilon_p, H_m\right)\dot{H}_m.\end{aligned} \tag{36}$$

Discarding $\bar{\mu}_{11}^0$ in equation (33), equations (35) and (36) yield the magnetic polarization M_k^{sp} according to equation (15) instead of B_k. This quantity is equivalent to M_k^{irr} in equation (14); however, a different notation is chosen due to the reversible characteristic of the magnetization in the phenomenological model. The specific magnetization m_k, which is commonly depicted in experimental plots, is finally obtained as

$$m_k = \mu_0^{-1}\varrho^{-1}M_k^{sp}, \tag{37}$$

where ϱ denotes the mass density of the material.

FE formulation

An approximate solution can be obtained applying the FE method. This requires the weak formulation of field equations which can be obtained, for example, from the generalized Hamilton's variational principle

$$\delta \int_{t_0}^{t_1} (K - \Psi) dt + \int_{t_0}^{t_1} \delta W^a dt = 0, \tag{38}$$

where K and δW^a denote kinetic energy and virtual work of the applied external forces, charges and normal magnetic flux, that is

$$\delta W^a = \int_S \left(t_i \delta u_i + \omega_s^{el} \delta \varphi^{el} + \omega_s^m \delta \varphi^m \right) dS \tag{39}$$

acting at the boundary S. The weak formulation is equivalent to the differential equation (6) as well as natural boundary conditions, if a potential $\Psi(\varepsilon_p, E_l, H_k)$ is inserted into equation (38) and the quasi-static case ($K = 0$) is chosen. In that case, Hamilton's principle equals the principle of the minimum of the total potential energy: $\delta\Pi = \delta(\Pi^i + \Pi^a) = 0$ with $\delta W^a = -\delta\Pi^a$ and $\Psi = \Pi^i$. In detail, the weak formulation is given as

$$\begin{aligned} &\int_V \left(\sigma_{ij} \delta u_{i,j} + D_k \delta \varphi^{el}_{,k} + B_l \delta \varphi^m_{,l} \right) dV - \int_S t_i \delta u_i dS \\ &+ \int_S \omega_s^{el} \delta \varphi^{el} dS + \int_S \omega_s^m \delta \varphi^m dS = 0, \end{aligned} \tag{40}$$

where V is the domain of the magnetoelectroelastic body.

For the phenomenological constitutive approach, the potential $\Psi(\varepsilon_p, E_l, H_k)$ is easily derived from $\bar{\Psi}(\sigma_p, E_l, H_k)$ according to equation (26) by the Legendre transformation

$$\Psi(\varepsilon_p, E_l, H_k) = \bar{\Psi}(\sigma_p, E_l, H_k) - \frac{\partial \bar{\Psi}}{\partial \sigma_p} \sigma_p = \bar{\Psi} + \varepsilon_p \sigma_p. \tag{41}$$

For the calculation of element matrices, the most general and efficient technique is the application of isoparametric FEs (Bathe, 2006). Displacements and potentials are approximated within each element using the interpolations

$$\begin{aligned} u_i &= \sum_{\alpha=1}^{N} h_u^\alpha u_i^\alpha = [h_u]\{u_i\}, \\ \varphi^{el} &= \sum_{\alpha=1}^{N} h_{el}^\alpha \varphi^{el^\alpha} = [h_{el}]\{\varphi^{el}\}, \\ \varphi^m &= \sum_{\alpha=1}^{N} h_m^\alpha \varphi^{m^\alpha} = [h_m]\{\varphi^m\}, \end{aligned} \tag{42}$$

where N is the number of nodes per element and $[h_u]$, $[h_{el}]$, and $[h_m]$ are isoparametric shape functions

$$\begin{aligned} [h_u] &= \begin{bmatrix} h_u^{(1)} & 0 & 0 & h_u^{(2)} & 0 & 0 & \dots & h_u^{(N)} & 0 & 0 \\ 0 & h_u^{(1)} & 0 & 0 & h_u^{(2)} & 0 & \dots & 0 & h_u^{(N)} & 0 \\ 0 & 0 & h_u^{(1)} & 0 & 0 & h_u^{(2)} & \dots & 0 & 0 & h_u^{(N)} \end{bmatrix} \\ [h_{el}] &= \left[h_{el}^{(1)} \quad h_{el}^{(2)} \quad \dots h_{el}^{(N)} \right], [h_m] = \left[h_m^{(1)} \quad h_m^{(2)} \quad \dots h_m^{(N)} \right]. \end{aligned} \tag{43}$$

The expressions for the electric and magnetic fields as well as mechanical strain are obtained by differentiating equation (42) with respect to the spatial coordinates x_i, relating the scalar potentials and displacements at nodes to the electric or magnetic fields and strain at the integration points of an element

$$\{\varepsilon\} = [B_u]\{u_i\}, \{E\} = -[B_{el}]\{\varphi^{el}\}, \{H\} = -[B_m]\{\varphi^m\} \tag{44}$$

Applying the fundamental lemma of variational calculus to equation (40), the partial stiffness matrices (mechanical, electric, magnetic, and the different mixed expressions) are obtained

$$\begin{aligned} [K_{uu}] &= \int_{(V)} [B_u]^T [c] [B_u] dV, \\ \left[K_{\varphi^{el}\varphi^{el}}\right] &= -\int_{(V)} [B_{el}]^T [\kappa]^T [B_{el}] dV, \\ \left[K_{\varphi^m\varphi^m}\right] &= -\int_{(V)} [B_m]^T [\mu]^T [B_m] dV, \\ \left[K_{u\varphi^m}\right] &= \int_{(V)} [B_u]^T [q]^T [B_m] dV. \end{aligned} \tag{45}$$

The material laws according to sections "Physically motivated ferromagnetic model" and "Phenomenologically motivated ferromagnetic model" are expressed by the matrices $[c]$, $[\kappa]$, $[\mu]$, and $[q]$.

The calculation of the generalized stiffness matrix requires numerical integration, for example, applying the Gauss quadrature. Finally, the boundary value problem is formulated as an algebraic system of equations $[K]\{U\} = \{R\}$

$$\begin{bmatrix} [K_{uu}] & [0] & \left[K_{u\varphi^m}\right] \\ [0] & \left[K_{\varphi^{el}\varphi^{el}}\right] & [0] \\ \left[K_{\varphi^m u}\right] & [0] & \left[K_{\varphi^m\varphi^m}\right] \end{bmatrix} \begin{Bmatrix} \{u_i\} \\ \{\varphi^{el}\} \\ \{\varphi^m\} \end{Bmatrix} = \begin{Bmatrix} \{F_s\} \\ \{Q_s^{el}\} \\ \{Q_s^m\} \end{Bmatrix} \tag{46}$$

where F_s, Q_s^{el}, and Q_s^m denote the forces and generalized charges at nodes

$$\{F_s\} = \int_S [h_u]^T \{t\} dS, \ \{Q_s^{el}\} = -\int_S [h_{el}]^T \omega_s^{el} dS,$$
$$\{Q_s^m\} = -\int_S [h_m]^T \omega_s^m dS. \quad (47)$$

The nonlinear irreversible ferromagnetic–dielectric model is based on the constitutive equation (14) inserting the irreversible quantities and material coefficients from the domain averaging equations (16), (24), and (25) taking into account the evolution law for domain volume fraction equation (20). Inserting the constitutive relations into the weak formulation equation (40) according to

$$\int_V \left\{ \delta u_{i,j} c_{ijkl} \left(\varepsilon_{kl} - \varepsilon_{kl}^{irr} \right) + \delta\varphi^m_{,k} \left[\mu_{km} H_m + M_k^{irr} \right] + \delta\varphi^{el}_{,l} \kappa_{ln} H_n \right\} dV$$
$$- \int_S t_i \delta u_i dS + \int_S \omega_s^m \delta\varphi^m dS + \int_S \omega_s^{el} \delta\varphi^{el} dS = 0, \quad (48)$$

and rearranging irreversible fields

$$\int_V \left\{ \delta u_{i,j} c_{ijkl} \varepsilon_{kl} + \delta\varphi^m_{,k} \mu_{km} H_m + \delta\varphi^{el}_{,l} \kappa_{ln} E_n \right\} dV$$
$$- \int_V \delta u_{i,j} c_{ijkl} \varepsilon_{kl}^{irr} dV + \int_V \delta\varphi^m_{,k} M_k^{irr} dV - \int_S t_i \delta u_i dS \quad (49)$$
$$+ \int_S \omega_s^m \delta\varphi^m dS + \int_S \omega_s^{el} \delta\varphi^{el} dS = 0$$

is obtained. The terms $c_{ijkl}\varepsilon_{kl}^{irr}$ and M_k^{irr} have to be interpreted as intrinsic stresses and magnetization due to Bloch wall motion.

For the physically motivated model, equation (46) is extended in the following way

$$\begin{bmatrix} [K_{uu}] & [0] & [K_{u\varphi^m}] \\ [0] & [K_{\varphi^{el}\varphi^{el}}] & [0] \\ [K_{\varphi^m u}] & [0] & [K_{\varphi^m \varphi^m}] \end{bmatrix} \begin{Bmatrix} \{u_i\} \\ \{\varphi^{el}\} \\ \{\varphi^m\} \end{Bmatrix} = \begin{Bmatrix} \{F_s\} + \{F_e\} \\ \{Q_s^{el}\} \\ \{Q_s^m\} + \{Q_e^m\} \end{Bmatrix}. \quad (50)$$

The additional nodal loads

$$\{F_e\} = \int_V [B_u]^T [c] \{\varepsilon^{irr}\} dV, \ \{Q_e^m\} = -\int_V [B_m]^T \{M^{irr}\} dV \quad (51)$$

account for the nonlinear irreversible contributions.

Concerning the numerical algorithm, where a Gauss quadrature scheme is applied for the integration within elements, it has to be noted that the intrinsic nodal loads according to equation (51) as well as the stiffness matrices depend on the load history. Therefore, an incremental procedure is inevitable where the material behavior is evaluated at each integration point, representing an RVE, and load step. Is domain wall motion initiated at one or more points, the stiffness matrices and intrinsic nodal loads have to be updated according to the evolution of internal variables, see equations (16), (24), and (25). Subsequently, the system of equation (50) is re-solved keeping external loads constant since resulting residual stresses and magnetization may initiate further domain jumping. This procedure is repeated until equilibrium is reached at all integration points whereupon the next external load step is introduced. Concerning the numerical parameter $d\nu_n^0$ according to equation (20), it ranges from 0.0025 to 0.01 where smaller values foster numerical stability, whereas larger values reduce computational costs.

Results

The two constitutive models according to section "Constitutive models of ferromagnetic materials" have been implemented within the framework of the FE method according to section "FE formulation." The material parameters are outlined in Appendix 1. Cobalt ferrite ($CoFe_2O_4$) is employed as an example to demonstrate nonlinear reversible behavior of soft magnetic materials, whereas AlNiCo 35/5 represents a hard magnetic alloy exhibiting pronounced hysteresis behavior.

In Figure 5, results from the microphysical model are shown in terms of magnetic polarization, induction, and strain versus magnetic field. According to equation (2), the induction B_k and the magnetic polarization M_k^{irr} differ in terms of $\mu_{km}H_m$, leading to an almost linear increase in B_k for large magnetic fields where M_k^{irr} is saturated. The dashed red line in the second quadrant emanates from experimental findings (Magnetfabrik Bonn GmbH, 2009) for the spontaneous magnetization M_k^{irr} (in Magnetfabrik Bonn GmbH, 2009, denoted as J) and is in very good agreement with the numerical prediction. The coercitivity of the polarization is slightly larger than that of the induction, while the remanences are equal. These features are likewise confirmed by experiments (Magnetfabrik Bonn GmbH, 2009), where the coercive values are given as $H_{cB} = 47\,\mathrm{kA/m}$ and $H_{cJ} = 48\,\mathrm{kA/m}$, respectively, and the remanent induction B_r as 1.12 T. Furthermore, a saturation of the magnetic polarization in terms of a horizontal tangent is observed for large magnetic fields above approximately 200 kA/m. The loading and unloading paths, however, are still slightly different, which is hardly visible compared to the strain due to the minor slope of the plot. Looking at the magnetostrictive effect illustrated in the right figure, the typical hysteresis behavior is observed with a remanent strain

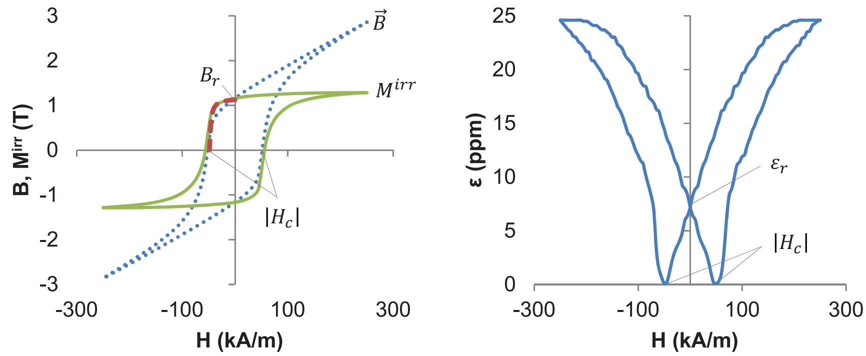

Figure 5. Numerical results for AlNiCo 35/5 from physically motivated model: magnetic induction and magnetic polarization, respectively (left; dashed red line: experimental data of demagnetization curve; Magnetfabrik Bonn GmbH, 2009) and strain versus magnetic field (right).

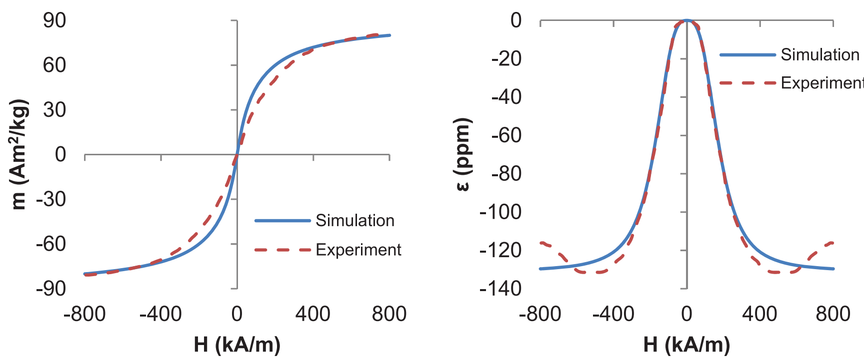

Figure 6. Experimental data (Bhame and Joy, 2006) and numerical results for the phenomenological ferromagnetic model: specific magnetization (left) and strain versus magnetic field (right) for $CoFe_2O_4$.

ε_r which, related to the maximum strain, is small compared to typical ferroelectric butterfly loops. In general, the values are much smaller than the parameter of spontaneous strain ε_D depicted in Table 3. The latter has to be understood as the saturated spontaneous strain of a single domain under ideal unclamped conditions, which is much larger than in a real polycrystalline material. There, residual stress and statistical domain orientations counteract the magnetic field. Apart from its physical interpretation, ε_D can be interpreted as one of very few model parameters of the microphysical approach.

In Figure 6, results are presented for the phenomenological model based on the simple approach equation (36) with constant values $\zeta_1 = \zeta_1^0$, $\zeta_2 = \zeta_2^0$, and $\xi = \xi^0$. As expected, the curves are nonlinear but reversible. They agree qualitatively with those in experiments. Cobalt ferrite is known to exhibit both hysteresis and reversible behaviors depending on the manufacturing conditions (Mohaideen and Joy, 2014). The specific magnetization m_k according to equation (37) in the left figure is determined with the density $\varrho = 5.3\,\mathrm{g/cm^3}$.

In Figure 7, the effect of a superimposed mechanical load on the ferromagnetic and magnetostrictive properties in terms of the magnetization or strain–magnetic field curves is investigated, based on the phenomenological constitutive model. In contrast to Figure 6, the more sophisticated approach has been applied, where ζ_1, ζ_2, and ξ depend on the stresses according to equation (34). The solid blue lines (b) represent a pure magnetic loading in the x_1-direction, whereas the other lines stand for the combined magnetomechanical loading. The lines with the negative values ε represent the strain ε_{11} along the axis of the magnetic field, whereas those with positive values ε represent the perpendicular strain ε_{22}. The plots are in agreement to what is expected intuitively. The tensile stress in the x_2-direction supports the magnetic field and leads to a saturation at lower magnetic loads, whereas a compressive stress in that direction acts contrariwise. A compressive stress in the direction of the magnetic field, however, supports the magnetic loading. Furthermore, the absolute values of the strain are larger in the direction of the magnetic field than perpendicular to it, that is, $|\varepsilon_{11}| > \varepsilon_{22}$.

As one application of the ferromagnetic–dielectric constitutive modeling, a magnetoelectric particle composite is investigated, consisting of a ferroelectric

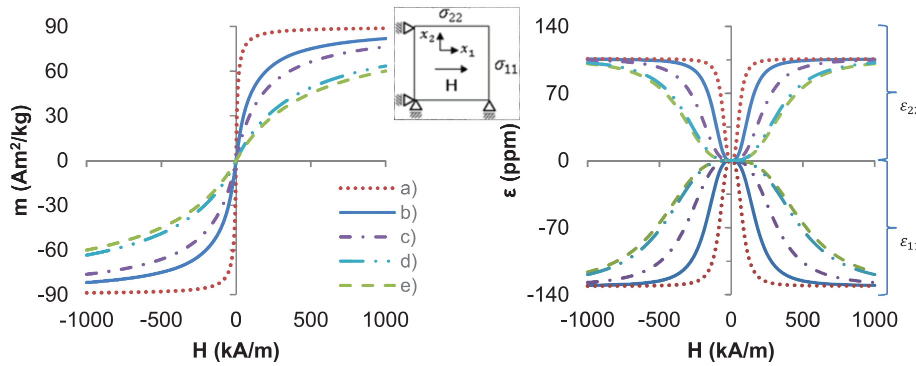

Figure 7. Numerical results for phenomenological ferromagnetic model at combined magnetomechanical loading: specific magnetization (left) and strain versus magnetic field (right) for $CoFe_2O_4$ at constant stress values of (a) $\sigma_{11} = 0$ MPa and $\sigma_{22} = 40$ MPa, (b) $\sigma_{11} = 0$ MPa and $\sigma_{22} = 0$ MPa, (c) $\sigma_{11} = 0$ MPa and $\sigma_{22} = -8$ MPa, (d) $\sigma_{11} = -8$ MPa and $\sigma_{22} = -40$ MPa, and (e) $\sigma_{11} = 0$ MPa and $\sigma_{22} = -40$ MPa.

matrix with a ferromagnetic inclusion. The goal of numerical simulations is, for example, to predict the magnetoelectric coupling coefficient, which is exploited in various engineering applications. In Avakian et al. (2015), similar composites have been investigated numerically, however, based on the assumption of linear magnetostrictive behavior. The first electric and/or magnetic loading cycle is of particular interest, leading to a poling of the initially unpoled material and being crucial for the functional properties and life time of the smart device. At this stage, nonlinear constitutive modeling is inevitable due to pronounced ferroelectric and ferromagnetic domain evolution. In the following simulations, the physically motivated ferromagnetic constitutive model equation (2) is applied to give a deeper insight into the domain arrangements during the poling process. The ferroelectric phase is described by equation (1).

A composite is considered with 80% $BaTiO_3$ as ferroelectric matrix including 20% of the hard ferromagnetic alloy AlNiCo 35/5, shaped as spherical particle. The FE model and boundary conditions as well as the loading scheme are shown in Figure 8. The material data of $BaTiO_3$ have been adopted from Avakian et al. (2015). The following numerical investigations are intended to be fundamental, rather than to provide engineering results, the model thus being restricted to just one single particle. In Figure 8(a), the boundary conditions for the poling and the magnetization processes, respectively, are illustrated. The cyclic electric and magnetic loads E_1 and H_1 are applied incrementally within the ranges $[0 - 5E_c]$ and $[0 - 5H_c]$ (see Figure 8(b)). While steps 1 and 2 represent the processes of poling and magnetization, step 3 is relevant for the determination of the magnetoelectric coupling coefficients g_{11} and g_{21}. The boundary conditions for the latter calculations are shown in Figure 8(c).

Keeping strain and stress, respectively, constant, two different definitions of the coupling coefficients are obtained, based on the thermodynamical potentials $\Psi(\varepsilon_{ij}, E_l, H_k)$ and $\bar{\Psi}(\sigma_{ij}, E_l, H_k)$, respectively

$$g_{n1}^{(\varepsilon)} = \left(\frac{\partial B_n}{\partial E_1}\right)_{\varepsilon_{ij}, H_l} \approx \frac{\Delta\langle B_n\rangle}{\Delta E_1^0}\bigg|_{\varepsilon_{ij}, H_l}, \; g_{n1}^{(\sigma)} = \left(\frac{\partial B_n}{\partial E_1}\right)_{\sigma_{ij}, H_l} \approx \frac{\Delta\langle B_n\rangle}{\Delta E_1^0}\bigg|_{\sigma_{ij}, H_l} \tag{52}$$

The electric potential difference in the x_1-direction $\bar{\varphi}^{el}$ yields the electric field E_1^0 which is imposed in the context of an electric Voigt assumption. The magnetic flux B_n in either x_1- or x_2-direction is obtained from the FE calculation, inserting the averages along the relevant edges into equation (52). The mechanical boundary conditions depicted in Figure 8(c) guarantee the constraints of constant strain (left figure) or constant stress (right figure) in the sense of an integral average in the RVE. The magnetic potential φ^m is zero at all edges, providing for a constant magnetic field in both directions.

In Figure 9, the polarization in the ferroelectric matrix and the magnetization in the ferromagnetic inclusion are shown at the end of the second load step (Figure 8(b)) where $E_1 = 0$. Here, the initialization or poling process is finished, and the composite is ready for magnetoelectric applications. A perfect alignment of polarization and magnetization with the poling fields cannot be expected. In fact, a noticeable scatter is anticipated, on one hand, due to the inhomogeneity of fields in the polycrystalline material. On the other hand, a partial depolarization is expected in the ferroelectric matrix due to the magnetic loading in combination with magnetostrictive and ferroelastic effects. The same holds for the ferromagnetic inclusion and the electric poling cycle. A favorable configuration is going along with a smallest possible scatter of local orientations of polarization and magnetization around the preferred direction. Second, the residual stresses, being responsible for cracking and thus for functional as well as structural degradation, are of interest. According to

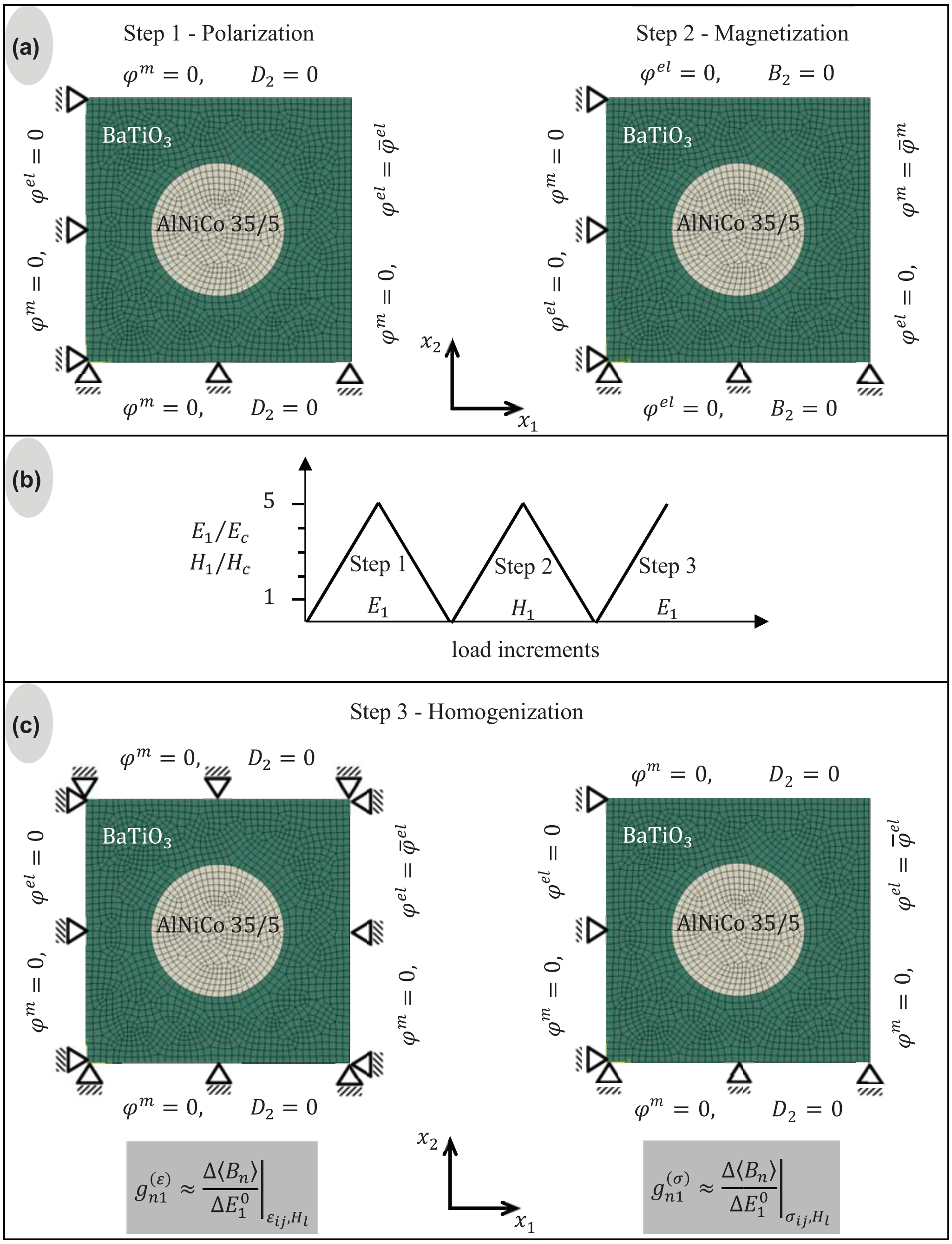

Figure 8. Magnetoelectric particle composite (matrix: $BaTiO_3$, particle: AlNiCo 35/5): (a) boundary conditions of the poling or magnetization process, (b) loading scheme, and (c) different boundary conditions for the calculation of the effective magnetoelectric coupling coefficients g_{11} and g_{21}.

Figure 9(a), the magnetization and polarization show a moderate scatter around the intended x_1-direction, leaving a sufficiently large potential for optimization. The tensile residual stresses, according to Figure 9(b), exhibit a maximum of approximately 100 MPa, certainly leading to cracking.

In Figure 10, some results of a first electric loading after the poling process (step 3 in Figure 8(b)) are illustrated in terms of maximum principal stress and magnetic induction at $E_1^0/E_c = 0.5$. The left picture shows the case with kinematic constraints, the right one represents traction free edges. The smaller figures in between are details for both boundary conditions and two locations. As expected, the kinematic constraint leads to significant compressive stress, while the free boundaries result in a stress distribution with predominantly tensile maximum principal stresses. The arrows indicate the vectors of the magnetic induction, exhibiting larger quantities in the ferromagnetic inclusion than in the ferromagnetic matrix, where the magnetic

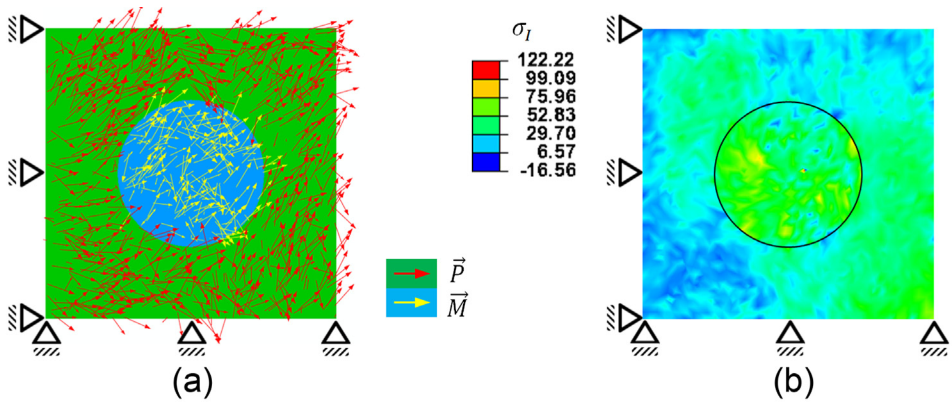

Figure 9. Polarized and magnetized magnetoelectric composite with AlNiCo 35/5—inclusion in a $BaTiO_3$—matrix (a) vectors of magnetization $\vec{M}$ and polarization $\vec{P}$ and (b) maximum principal stress σ_1 (MPa).

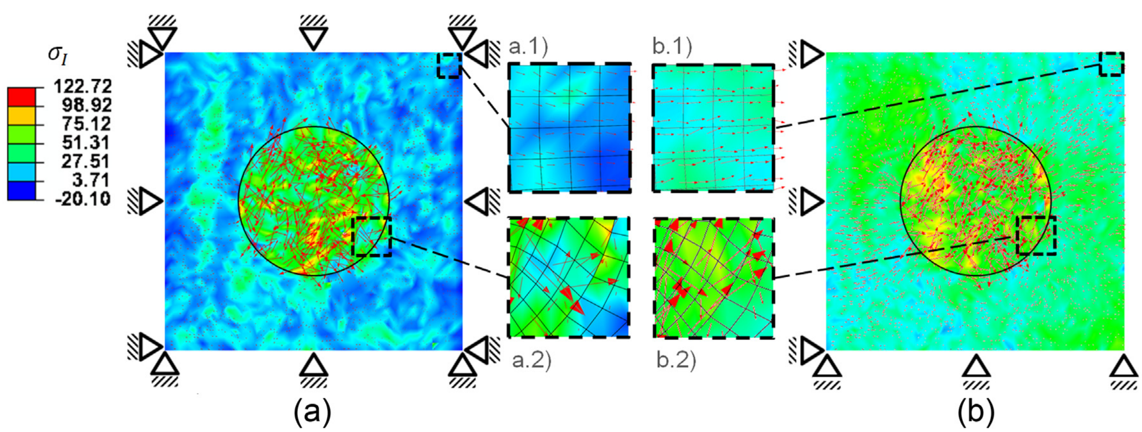

Figure 10. Vectors of magnetic induction $\vec{B}$ and maximum principal stress σ_1 (MPa) for a polarized and magnetized magnetoelectric composite with AlNiCo 35/5—inclusion in a $BaTiO_3$—matrix under electric loading of $0.5E_c$, (a) constant strain and (b) constant stress boundary conditions.

permeability is much smaller. The local directions of the magnetic flux are clearly determined by the poling and loading fields, respectively. Due to the compression in the constrained case, the magnetization of the ferromagnetic phase is considerably reduced, which is obvious comparing a.2 and b.2 in Figure 10. The density of arrows is a measure of the absolute quantity of magnetization since FE integration points without any visible arrow indicate a vanishing magnetization at that point. Similarly, the magnetic induction at the edges of the FE model is much smaller for the constrained case than for the unconstrained one, becoming obvious from a comparison of a.1 and b.1 in Figure 10.

This feature is further illustrated in Figure 11, where the coordinates of the magnetic induction B_1 and B_2 are plotted versus the normalized electric field using solid lines. While the magnitude for the constant average stress $B_1^{(\sigma)} \approx |\vec{B}|$ remains unchanged below $2.5E_c$, slightly decreasing for larger electric loads, the one for constant strain $B_n^{(\varepsilon)}$ exhibits a steep gradient below $0.5E_c$. As one consequence, the magnetoelectric coupling coefficients g_{n1}, according to equation (52) being the derivatives of the magnetic induction, show narrow negative peaks at low electric loads for the constant strain boundary condition, that is, $g_{n1}^{(\varepsilon)}$.

In Figure 12, the magnetoelectric coupling coefficients $g_{n1}^{(\sigma)}$ for the unconstrained boundary value problem according to Figure 8(c) are once more plotted versus the normalized electric field. In contrast to Figure 11, the scaling of the ordinate has been refined, in order to show details of the graphs. The coupling coefficients prove to be predominantly negative in the investigated case of an electric field in the poling direction. The maximum absolute value is obtained for g_{11}. The average magnitude is approximately $-6E-9\,\mathrm{N\,s/V\,C}$. The large oscillations in Figure 12 might be unexpected at the first glance. The B-field has to be subject to fluctuations when increasing the E-field due to ferroelectric domain switching and Barkhausen

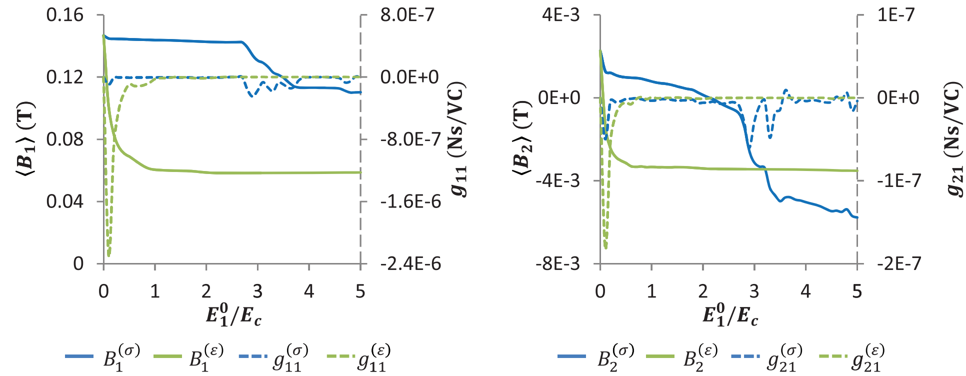

Figure 11. Magnetoelectric coupling coefficients and magnetic induction versus normalized electric load after poling process.

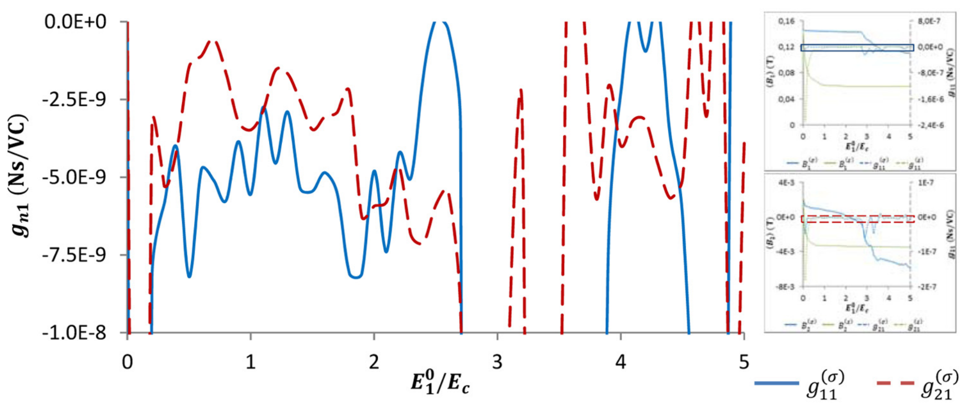

Figure 12. Magnetoelectric coupling coefficients versus normalized electric load after poling process.

jumping occurring very discontinuously both spatially and chronologically. The magnetoelectric coupling coefficients mathematically and physically being the derivative thus have to be highly fluctuant.

Conclusion

Two types of constitutive models for ferromagnetic materials have been presented. The one is based on physical considerations on the micro- and mesolevels; the other is purely phenomenological. The one produces irreversible hysteresis behavior, and the other exhibits nonlinear reversible features. Both characteristics are well known from different ferromagnetic materials. Due to intended applications of the models with respect to multiferroic composites, dielectric properties are included in both constitutive approaches. The material models have been implemented within an FE context to be able to investigate complex boundary value problems. Verifications of the constitutive models under combined magnetomechanical loading demonstrate their capability of describing ferromagnetic material behavior appropriately. Finally, a multiferroic composite, consisting of a ferromagnetic inclusion in a ferroelectric matrix, has been investigated numerically, applying physically motivated constitutive models for both phases. Polarization and magnetization of an initially unpoled composite have been simulated, being the basis for the prediction of magnetoelectric coupling coefficients for different mechanical boundary conditions.

Declaration of Conflicting Interests

The author(s) declared no potential conflicts of interest with respect to the research, authorship, and/or publication of this article.

Funding

The author(s) received no financial support for the research, authorship, and/or publication of this article.

References

Aboudi J (2001) Micromechanical analysis of fully coupled electro-magneto-thermo-elastic multiphase composites. *Smart Materials and Structures* 10(5): 867–877.

Adly AA, Mayergoyz ID and Bergqvist A (1991) Preisach modeling of magnetostrictive hysteresis. *Journal of Applied Physics* 69(8): 5777–5779.

Armstrong WD (1997) Magnetization and magnetostriction processes in Tb(0.27-0.30)Dy(0.73-0.70)Fe(1.9-2.0). *Journal of Applied Physics* 81(5): 2321–2326.

Armstrong WD (2003) An incremental theory of magneto-elastic hysteresis in pseudo-cubic ferro-magnetostrictive alloys. *Journal of Magnetism and Magnetic Materials* 263: 208–218.

Atulasimha J, Flatau AB and Summers E (2007) Characterization and energy-based model of the magnetomechanical behavior of polycrystalline iron-gallium alloys. *Smart Materials and Structures* 16(4): 1265–1276.

Avakian A, Gellmann R and Ricoeur A (2015) Nonlinear modeling and finite element simulation of magnetoelectric coupling and residual stress in multiferroic composites. *Acta Mechanica* 226(8): 2789–2806.

Bathe KJ (2006) *Finite Elemente Methoden*. Berlin: Prentice Hall.

Benveniste Y (1995) Magnetoelectric effect in fibrous composites with piezoelectric and piezomagnetic phases. *Physical Review B* 51(22): 16424–16427.

Bergmann L and Schaefer C (2005) *Lehrbuch der Experimentalphysik. Vol. 6: Festkorper*. Berlin/New York: De Gruyter.

Bergqvist AJ (1996) A simple vector generalization of the Jiles-Atherton model of hysteresis. *IEEE Transactions on Magnetics* 32(5): 4213–4215.

Bergqvist AJ and Engdahl G (1991) A stress-dependent magnetic Preisach hysteresis model. *IEEE Transactions on Magnetics* 27(6): 4796–4798.

Bhame SD and Joy PA (2006) Tuning of the magnetostrictive properties of $CoFe_2O_4$ by Mn substitution for Co. *Journal of Applied Physics* 100(11): 113911.

Bhame SD and Joy PA (2007) Magnetic and magnetostrictive properties of manganese substituted cobalt ferrite. *Journal of Physics D: Applied Physics* 40(11): 3263–3267.

Bhame SD and Joy PA (2008) Effect of sintering conditions and microstructure on the magnetostrictive properties of cobalt ferrite. *Journal of the American Ceramic Society* 91(6): 1976–1980.

Bibes M and Barthélémy A (2008) Multiferroics: towards a magnetoelectric memory. *Nature Materials* 7(6): 425–426.

Borgohain C, Senapati KK, Mishra D, et al. (2010) A new $CoFe_2O_4$–Cr_2O_3–SiO_2 fluorescent magnetic nanocomposite. *Nanoscale* 2(10): 2250–2256.

Bozorth RM (1951) *Ferromagnetism*. New York: Van Nostrand.

Buchanan GR (2004) Layered versus multiphase magneto-electro-elastic composites. *Composites Part B: Engineering* 35(5): 413–420.

Cardelli E, Della Torre E and Pinzaglia E (2004) Identifying the parameters of the reduced vector Preisach model: Theory and experiment. *IEEE Transactions on Magnetics* 40(4): 2164–2166.

Carman GP and Mitrovic M (1995) Nonlinear constitutive relations for magnetostrictive materials with applications to 1-D problems. *Journal of Intelligent Material Systems and Structures* 6(5): 673–683.

Chen PJ and Tucker TJ (1981) Determination of the polar equilibrium properties of the ferroelectric ceramic PZT 65/35. *Acta Mechanica* 38 (3–4): 209–218.

Cocks ACF and McMeeking RM (1999) A phenomenological constitutive law for the behaviour of ferroelectric ceramics. *Ferroelectrics* 228(1): 219–228.

Concas G, Spano G, Cannas C, et al. (2009) Inversion degree and saturation magnetization of different nanocrystalline cobalt ferrites. *Journal of Magnetism and Magnetic Materials* 321(12): 1893–1897.

Dapino MJ, Smith RC and Flatau AB (2000) Structural magnetic strain model for magnetostrictive transducers. *IEEE Transactions on Magnetics* 36(3): 545–556.

Du Trémolet de Lacheisserie E, Gignoux D and Schlenker M (2005) *Magnetism: Materials and Applications*. New York: Springer.

Eerenstein W, Wiora M, Prieto J, et al. (2007) Giant sharp and persistent converse magnetoelectric effects in multiferroic epitaxial heterostructures. *Nature Materials* 6(5): 348–351.

El-Okr MM, Salem MA, Salim MS, et al. (2011) Synthesis of cobalt ferrite nano-particles and their magnetic characterization. *Journal of Magnetism and Magnetic Materials* 323(7): 920–926.

Entel P, Buchelnikov VD, Khovailo VV, et al. (2006) Modelling the phase diagram of magnetic shape memory Heusler alloys. *Journal of Physics D: Applied Physics* 39(5): 865–889.

Etier MF, Shvartsman VV, Stromberg F, et al. (2012) Synthesis and magnetic properties of cobalt ferrite nanoparticles. In: *MRS Proceedings 1398: 2011 MRS fall meeting and exhibit* (Symposium Q: magnetoelectric composites), Boston, MA, 28 November–2 December.

Evans PG and Dapino MJ (2010) Efficient magnetic hysteresis model for field and stress application in magnetostrictive Galfenol. *Journal of Applied Physics* 107(6): 063906.

Feltin N and Pileni MP (1997) New technique for synthesizing iron ferrite magnetic nanosized particles. *Langmuir* 13(15): 3927–3933.

Fiebig M (2005) Revival of the magnetoelectric effect. *Journal of Physics D: Applied Physics* 38(8): R123–R152.

Harshe G, Dougherty JO and Newnham RE (1993) Theoretical modelling of multilayer magnetoelectric composites. *International Journal of Applied Electromagnetics in Materials* 4: 145–159.

Hill N (2000) Why are there so few magnetic ferroelectrics? *Journal of Physical Chemistry B* 104(29): 6694–6709.

Huang JH and Kuo WS (1997) The analysis of piezoelectric/piezomagnetic composite materials containing ellipsoidal inclusions. *Journal of Applied Physics* 81(3): 1378–1386.

Hwang SC, Lynch CS and McMeeking RM (1995) Ferroelectric/ferroelastic interactions and a polarization switching model. *Acta Metallurgica et Materialia* 43(5): 2073–2084.

Jackson JD (1998) *Classical Electrodynamics*. New York: John Wiley & Sons.

Jiles DC (1995) *Introduction to Magnetism and Magnetic Materials*. London: Chapman & Hall.

Kádár G (1987) On the Preisach function of ferromagnetic hysteresis. *Journal of Applied Physics* 61(8): 4013–4015.

Kamlah M, Liskowsky AC, McMeeking RM, et al. (2005) Finite element simulation of a polycrystalline ferroelectric based on a multidomain single crystal switching model. *International Journal of Solids and Structures* 42(9–10): 2949–2964.

Kellogg RA, Flatau A, Clark AE, et al. (2005) Quasi-static transduction characterization of Galfenol. *Journal of Intelligent Material Systems and Structures* 16(6): 471–479.

Kessler H and Balke H (2001) On the local and average energy release in polarization switching phenomena. *Journal of the Mechanics and Physics of Solids* 49(5): 953–978.

Kiefer B and Lagoudas DC (2004) Phenomenological modeling of ferromagnetic shape memory alloys. In: *SPIE 5387, smart structures and materials 2004: active materials: behavior and mechanics*, San Diego, CA, 14 March, pp. 164–176. Bellingham, WA: SPIE.

Kittel C (2006) *Einführung in die Festkörperphysik*, vol. 14. München: Oldenbourg.

Koyama T (2008) Phase-field modeling of microstructure evolutions in magnetic materials. *Science and Technology of Advanced Materials* 9(1): 013006.

Koyama T and Onodera H (2003) Phase-field simulation of microstructure changes in Ni_2MnGa ferromagnetic alloy under external stress and magnetic fields. *Materials Transactions* 44(12): 2503–2508.

Krantz MC and Gerken M (2013) Theory of magnetoelectric effect in multilayer nanocomposites on a substrate: resonant bending-mode response. *AIP Advances* 3(5): 052131.

Kuo HY, Slinger A and Bhattacharya K (2010) Optimization of magnetoelectricity in piezoelectric–magnetostrictive bilayers. *Smart Materials and Structures* 19(12): 125010–125022.

Labusch M, Etier M, Lupascu DC, et al. (2014) Product properties of a two-phase magneto-electric composite: synthesis and numerical modeling. *Computational Mechanics* 54(1): 71–83.

Lange S and Ricoeur A (2015) A condensed microelectromechanical approach for modeling tetragonal ferroelectrics. *International Journal of Solids and Structures* 54: 100–110.

Lee J, Boyd JG and Lagoudas DC (2005) Effective properties of three-phase electro-magneto-elastic composites. *International Journal of Engineering Science* 43(10): 790–825.

Lee SJ, Lo CCH, Matlage PN, et al. (2007) Magnetic and magnetoelastic properties of Cr-substituted cobalt ferrite. *Journal of Applied Physics* 102(7): 073910.

Li JY (2000) Magnetoelectroelastic multi-inclusion and inhomogeneity problems and their applications in composite materials. *International Journal of Engineering Science* 38(18): 1993–2011.

Li JY and Dunn ML (1998) Micromechanics of magnetoelectroelastic composite materials: average fields and effective behavior. *Journal of Intelligent Material Systems and Structures* 9(6): 404–416.

Linnemann K, Klinkel S and Wagner W (2009) A constitutive model for magnetostrictive and piezoelectric materials. *International Journal of Solids and Structures* 46: 1149–1166.

Lu AH, Salabas EL and Schüth F (2007) Magnetic nanoparticles: synthesis, protection, functionalization, and application. *Angewandte Chemie: International Edition* 46(8): 1222–1244.

Lu XY, Li H and Wang B (2011) Theoretical analysis of electric, magnetic and magnetoelectric properties of nanostructured multiferroic composites. *Journal of the Mechanics and Physics of Solids* 59(10): 1966–1977.

Lu XY, Wang B, Zheng Y, et al. (2009) Phenomenological theory of 1–3 type multiferroic composite thin film: thickness effect. *Journal of Physics D: Applied Physics* 42(1): 15309.

Ma FD, Jin YM, Wang YU, et al. (2014) Effect of magnetic domain structure on longitudinal and transverse magnetoelectric response of particulate magnetostrictive-piezoelectric composites. *Applied Physics Letters* 104(11): 112903.

McCallum RW, Dennis KW, Jiles DC, et al. (2001) Composite magnetostrictive materials for advanced automotive magnetomechanical sensors. *Low Temperature Physics* 27(4): 266–274.

Magnetfabrik Bonn GmbH (2009) *AlNiCo 500: DIN-Characterization 35/5*. Bonn: Magnetfabrik Bonn GmbH.

Mayergoyz ID and Friedman G (1987) Isotropic vector Preisach model of hysteresis. *Journal of Applied Physics* 61(8): 4022–4024.

Miehe C and Ethiraj G (2012) A geometrically consistent incremental variational formulation for phase field models in micromagnetics. *Computer Methods in Applied Mechanics and Engineering* 245–246: 331–347.

Miehe C, Kiefer B and Rosato D (2011a) An incremental variational formulation of dissipative magnetostriction at the macroscopic continuum level. *International Journal of Solids and Structures* 48(13): 1846–1866.

Miehe C, Rosato D and Kiefer B (2011b) Variational principles in dissipative electro-magneto-mechanics: a framework for the macro-modeling of functional materials. *International Journal for Numerical Methods in Engineering* 86(10): 1225–1276.

Mohaideen KK and Joy PA (2014) Studies on the effect of sintering conditions on the magnetostriction characteristics of cobalt ferrite derived from nanocrystalline powders. *Journal of the European Ceramic Society* 34(3): 677–686.

Morrish AH (2001) *The Physical Principles of Magnetism*. New York: IEEE Press.

Nan CW (1994) Magnetoelectric effect in composites of piezoelectric and piezomagnetic phases. *Physical Review B* 50(9): 6082–6088.

Nan CW, Bichurin MI, Dong SX, et al. (2008) Multiferroic magnetoelectric composites: historical perspective, status, and future directions. *Journal of Applied Physics* 103(3): 031101.

Parton VZ and Kudryavtsev BA (1988) *Electromagnetoelasticity: Piezoelectrics and Electrically Conductive Solids*. New York: Gordon and Breach Science Publishers.

Plassmann W (2013) *Handbuch Elektrotechnik: Grundlagen und Anwendungen für Elektrotechniker*. 6th Aufl. Wiesbaden: Springer.

Preisach F (1935) Über die magnetische Nachwirkung. *Zeitschrift für Physik* 94: 277–302.

Rajendran M, Pullar RC, Bhattacharya AK, et al. (2001) Magnetic properties of nanocrystalline $CoFe_2O_4$ powders prepared at room temperature: variation with crystallite size. *Journal of Magnetism and Magnetic Materials* 232(1–2): 71–83.

Ramesh R and Spaldin N (2007) Multiferroics: progress and prospects in thin films. *Nature Materials* 6(1): 21–29.

Restorff JB, Savage HT, Clark AE, et al. (1990) Preisach modeling of hysteresis in Terfenol. *Journal of Applied Physics* 67(9): 5016–5018.

Schmid H (1994) Multi-ferroic magnetoelectrics. *Ferroelectrics* 162(1): 317–338.

Scott JF (2007) Data storage: multiferroic memories. *Nature Materials* 6(4): 256–257.

Shi Y, Ding J and Yin H (2000) $CoFe_2O_4$ nanoparticles prepared by the mechanochemical method. *Journal of Alloys and Compounds* 308(1–2): 290–295.

Smith RC and Dapino MJ (2006) A homogenized energy model for the direct magnetomechanical effect. *IEEE Transactions on Magnetics* 42(8): 1944–1957.
Smith RC, Seelecke S, Dapino MJ, et al. (2006) A unified framework for modeling hysteresis in ferroic materials. *Journal of the Mechanics and Physics of Solids* 54: 46–85.
Stefanita CG (2012) *Magnetism: Basics and Applications*. Heidelberg, New York: Springer.
Tang T and Yu W (2009) Micromechanical modeling of the multiphysical behavior of smart materials using the variational asymptotic method. *Smart Materials and Structures* 18(12): 125026.
Van Suchtelen J (1972) Product properties: a new application of composite materials. *Philips Research Reports* 27(1): 28–37.
Vanderlinde J (2005) *Classical Electromagnetic Theory*. Dordrecht: Springer.
Wan Y, Fang D and Hwang KC (2003) Non-linear constitutive relations for magnetostrictive materials. *International Journal of Non-Linear Mechanics* 38(7): 1053–1065.
Wan YP and Zhong Z (2004) Vibration analysis of Tb-Dy-Fe magnetostriction actuator and transducer. *Mechanics and Materials in Design* 1: 95–107.
Xu H, Pei Y, Fang D, et al. (2013) An energy-based dynamic loss hysteresis model for giant magnetostrictive materials. *International Journal of Solids and Structures* 50(5): 672–679.
Zayak AT, Buchelnikov VD and Entel P (2002) A Ginzburg-Landau theory for Ni-Mn-Ga. *Phase Transitions* 75(1–2): 243–256.
Zheng XJ and Liu XE (2005) A nonlinear constitutive model for Terfenol-D rods. *Journal of Applied Physics* 97: 053901.

Appendix 1

The coefficients of cobalt ferrite are found in Li and Dunn (1998) as well as Tang and Yu (2009) and listed in Table 1.

Additionally, the quantities in Table 2 have been identified for the phenomenological model.

Moreover, the quantities in Table 3 have been applied for the physically motivated model.

Due to the lack of elastic and dielectric constants in the literature, the values in Table 1 have been taken for AlNiCo 35/5 as well, assuming the same orders of magnitude.

Table 1. Material properties of $CoFe_2O_4$.

	$CoFe_2O_4$
c_{11} (GPa)	269.5
c_{12} (GPa)	170
c_{22} (GPa)	286
c_{23} (GPa)	173
c_{44} (GPa)	45.3
κ_{11} (C/Vm)	0.093E − 9
κ_{22}(C/Vm)	0.08E − 9

Table 2. Parameters of the phenomenological model adapted to the constitutive behavior of $CoFe_2O_4$.

Parameter	Unit	$CoFe_2O_4$
η_1	–	−131E − 6
η_2	–	106E − 6
ζ_1^0	A^3/m^3	5.5E + 15
ζ_2^0	A^3/m^3	2.1E + 15
ζ_1^σ	A^3/N m	3E + 9
$\zeta_2^\sigma = \zeta_1^\sigma(\zeta_2^0/\zeta_1^0)$	A^3/Nm	1.145E + 9
ρ	T	0.6
ξ^0	N/Vs	1E + 5
ξ^σ	m^2/Vs	1E − 2

Table 3. Parameters of the physically based model adapted to the constitutive behavior of AlNiCo 35/5 (Plassmann, 2013).

Parameter	Unit	Meaning	AlNiCo35/5
$H_c = H_{cB}$	kA/m	Coercivity of magnetic induction	47
μ^r	–	Relative recoil permeability	5
M^0	T	Magnitude of spontaneous magnetization	1.85
ε_D	–	Magnitude of spontaneous strain	0.04

μ^r is denoted in Plassmann (2013), as μ_{rec}.